Stem Cell Reports
Article

ISSCR

OPEN ACCESS

Lineage-specific dynamics of loss of X upregulation during inactive-X reactivation

Hemant Chandru Naik,[1] Deepshikha Chandel,[1] Sudeshna Majumdar,[1,4] Maniteja Arava,[1,5] Runumi Baro,[1] Harshavardhan BV,[1,2,3] Kishore Hari,[2] Parichitran Ayyamperumal,[1] Avinchal Manhas,[1] Mohit Kumar Jolly,[2] and Srimonta Gayen[1,6,*]

[1]Chromatin, RNA and Genome Laboratory, Department of Developmental Biology and Genetics, Indian Institute of Science, Bangalore 560012, India
[2]Department of Bioengineering, Indian Institute of Science, Bangalore 560012, India
[3]IISc Mathematics Initiative (IMI), Indian Institute of Science, Bangalore 560012, India
[4]Present address: Cell Biology of Genomes, National Cancer Institute, National Institutes of Health, Bethesda, MD 20892, USA
[5]Present address: Division of Genetics and Genomics, Center for Life Sciences, Boston Children's Hospital, Harvard Medical School, Boston 02115, USA
[6]Lead contact
*Correspondence: srimonta@iisc.ac.in
https://doi.org/10.1016/j.stemcr.2024.10.001

SUMMARY

In mammals, X chromosome dosage is balanced between sexes through the silencing of one X chromosome in females. Recent single-cell RNA sequencing analysis demonstrated that the inactivation of the X chromosome is accompanied by the upregulation of the active X chromosome (Xa) during mouse embryogenesis. Here, we have investigated if the reactivation of inactive-X (Xi) leads to the loss of Xa upregulation in different cellular or developmental contexts. We find that while Xi reactivation and loss of Xa upregulation are tightly coupled in mouse embryonic epiblast and induced pluripotent stem cells, that is not the case in germ cells. Moreover, we demonstrate that partial reactivation of Xi in mouse extra-embryonic endoderm stem cells and human B cells does not result in the loss of Xa upregulation. Finally, we have established a mathematical model for the transcriptional coordination of two X chromosomes. Together, we conclude that the reactivation of Xi is not always synchronized with the loss of Xa upregulation.

INTRODUCTION

X-linked genes play a crucial role in the development and cell fate specification (Cloutier et al., 2022; Marahrens et al., 1997; Schulz et al., 2014; Zhang et al., 2016). In therian female mammals, one of the X chromosomes is inactivated to compensate for the dosage of X-linked gene expression between sexes (Lyon, 1961). Therefore, X-linked genes are monoallelically expressed in both sexes compared to the biallelic autosomal expression. To balance the X-linked gene dosage relative to autosomal genes, genes on the active-X (Xa) undergo upregulation. The concept of X chromosome upregulation (XCU) was first hypothesized by Ohno in 1967 (Ohno S, 1967). As per Ohno, during the evolution of sex chromosomes, the Y chromosome degraded, which led to a dosage imbalance between X and autosomal genes, which was rectified through the upregulation of X chromosome (Graves, 2016; Ohno S, 1967). Subsequently, to counteract the overexpression of X-linked genes due to this upregulation, females evolved X chromosome inactivation (XCI). However, the existence of XCU remained contested for a long time. The first evidence of XCU was documented through microarray-based studies (Nguyen et al., 2006; Gupta et al., 2006; Lin et al., 2007, 2011). Subsequently, many studies confirmed the presence of XCU (Borensztein et al., 2017a; Cidral et al., 2021; Deng et al., 2011, 2013; Kharchenko et al., 2011; Larsson et al., 2019; Li et al., 2017; Lyu et al., 2022; Mahadevaiah et al., 2020; Mandal et al., 2020; De Mello et al., 2017; Pessia et al., 2012; Sangrithi et al., 2017; Wang et al., 2016; Yildirim et al., 2012). However, some studies refuted the existence of such XCU (Chen et al., 2020; Lin et al., 2012; Wang et al., 2017; Xiong et al., 2010; Yang and Chen, 2019). Recently, Lentini et al., using allele-resolved single-cell RNA sequencing (scRNA-seq) analysis, showed that XCU and XCI occur in a coordinated manner during early embryogenesis (Lentini et al., 2022). Subsequently, we also demonstrated such coordination between two X chromosomes in pre-gastrulating mouse embryos (Naik et al., 2022). In fact, it was shown that reactivation of the inactive-X (Xi) in inner cell mass (ICM) of blastocyst or mouse embryonic stem cells (mESCs) leads to the loss of Xa upregulation (Larsson et al., 2019; Lentini et al., 2022). However, whether such coordination between two X chromosomes in female cells is a universal phenomenon or restricted to certain developmental windows or cell types remains underexplored. In this study, we have explored the kinetics of loss of Xa upregulation upon Xi reactivation in different developmental or cellular contexts and show that loss of Xa upregulation is not always synchronized with Xi reactivation.

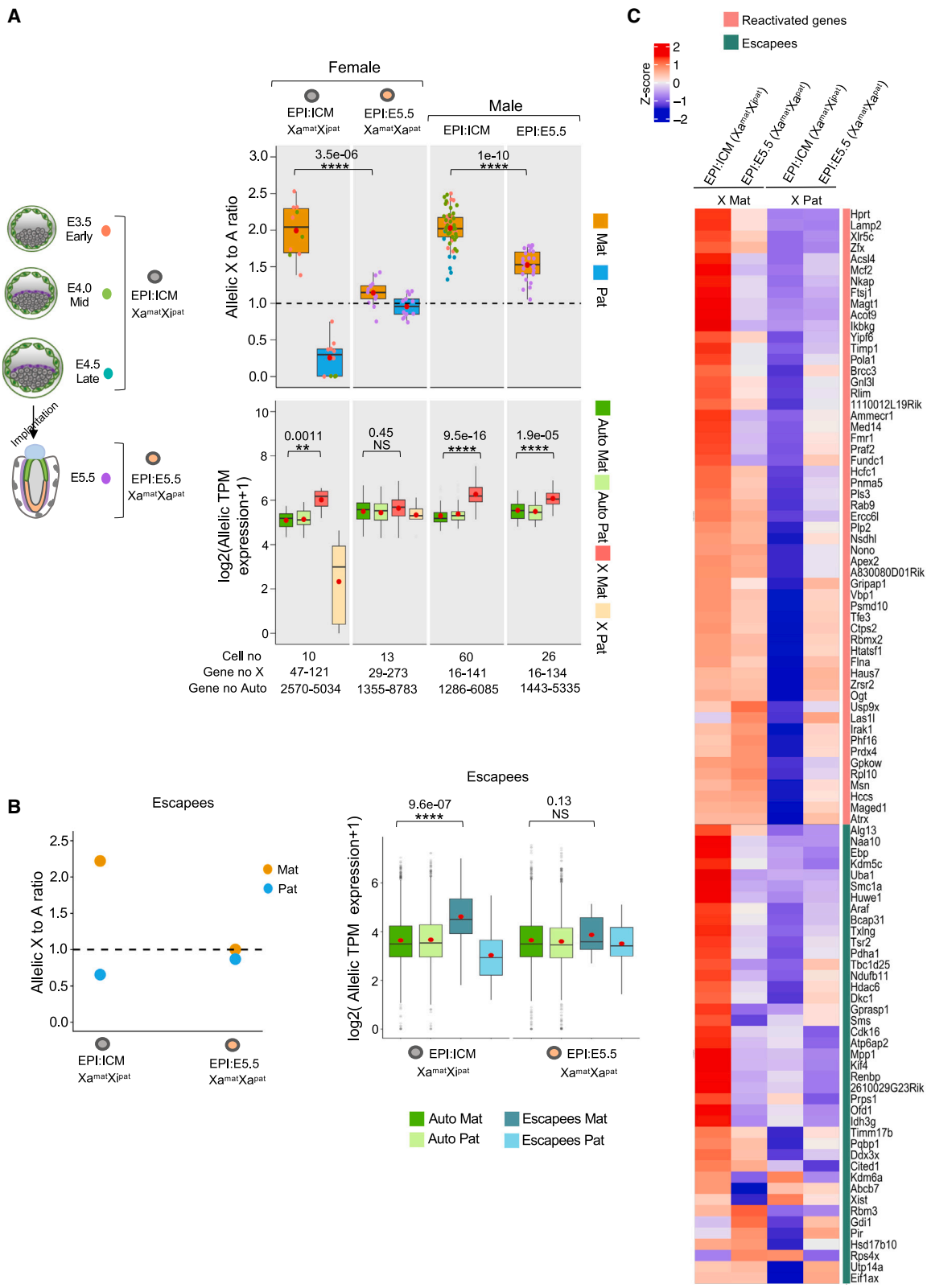

(legend on next page)

RESULTS

Loss of Xa upregulation upon reactivation of Xi in mouse embryonic epiblast

In mice, XCI happens in two phases: initially imprinted XCI in pre-implantation embryos, where paternal-X gets inactivated (Xi^{pat}) and later switches to random XCI in the post-implantation epiblast (Huynh and Lee, 2003; Lyon, 1961; Okamoto et al., 2004; Takagi and Sasaki, 1975). Switching of imprinted to random XCI is mediated through the reactivation of the imprinted Xi in the epiblast cells (Mak et al., 2004; Okamoto et al., 2004). We explored Xa expression dynamics during the initiation of imprinted XCI by profiling allele-specific gene expression at different stages of mouse pre-implantation embryos using available scRNA-seq datasets (Figure S1A). These embryos harbored polymorphic sites across their genome as they were derived from two diverged mouse strains: C57BL/6J (C57) and *Mus castaneous* (cast), which allowed us to perform allele-specific gene expression analysis (Figure S1A). We excluded low-expressed genes (<1 TPM) from our analysis. First, we presumably segregated cells of female embryos based on their XCI status: cells with no XCI ($Xa^{mat}Xa^{pat}$), partial XCI ($Xa^{mat}Xp^{pat}$), and complete XCI ($Xa^{mat}Xi^{pat}$) through profiling fraction expression from maternal Xa (Xa^{mat}) (Figure S1B). As expected, in male cells, we found expression of X-linked genes from the maternal allele only (Figure S1B). Additionally, autosomal genes had equivalent allelic expression from the paternal and maternal alleles, thereby validating our allele-specific expression analysis methodology (Figure S1B). Similarly, we observed the expression of Xist from the Xi^{pat} allele only in pre-implantation embryos (Figure S1C). Next, we explored the dynamics of Xa^{mat} upregulation upon the initiation of XCI through profiling allelic X to autosomal (A) gene expression ratio. X:A ratio is used as an indicator for the presence of XCU. If there is upregulation from Xa^{mat}, the expected Xa^{mat}:A^{mat} ratio should be >1 and close to 2. We found that Xa^{mat}:A^{mat} ratio and Xa^{pat}:A^{pat} ratio in $Xa^{mat}Xa^{pat}$ cells was almost equivalent and greater than 1, indicating overall higher X-linked expression than the autosomal genes during pre-implantation development (Figure S1D). As expected, we found that in $Xa^{mat}Xp^{pat}$ cells, Xa^{pat}:A^{pat} ratio tends to be down and reaches almost none in $Xa^{mat}Xi^{pat}$ XaXi cells, indicating inactivation of the paternal-X (Figure S1D). Interestingly, we found that the Xa^{mat}:A^{mat} ratio increased significantly in $Xa^{mat}Xp^{pat}$ and $Xa^{mat}Xi^{pat}$ cells compared to $Xa^{mat}Xa^{pat}$ cells, indicating concomitant upregulation of Xa upon XCI (Figure S1D). Similarly, we found that the Xa^{mat}:A^{mat} ratio in male cells was close to 2, indicating the presence of Xa upregulation (Figure S1D). Next, we profiled the Xa upregulation directly by analyzing the allelic expression pattern of autosomes and X chromosomes and found that Xa expression in female $Xa^{mat}Xp^{pat}$/$Xa^{mat}Xi^{pat}$ cells and male cells is significantly higher compared to the autosomal allelic expression, corroborating the Xa upregulation (Figure S1D). To eliminate the effect of gene expression variation in the scRNA-seq dataset, we performed the aforementioned analysis using common gene sets among $Xa^{mat}Xa^{pat}$, $Xa^{mat}Xp^{pat}$, and $Xa^{mat}Xi^{pat}$ cells and found a similar trend of Xa upregulation (Figures S1E and S1F). Moreover, analysis through different stages of mouse pre-implantation embryos also showed a similar pattern (Figure S1G). Altogether, in line with previous findings, we conclude that upon XCI, concomitant Xa upregulation balances the X-linked gene dosage relative to autosomal genes in mouse pre-implantation embryos (Lentini et al., 2022).

Next, we investigated if the reactivation of Xi leads to the loss of X upregulation in epiblast cells transitioning from imprinted to random X inactivation. We identified epiblast cells of ICM (EPI:ICM) from blastocysts (E3.5, E4.0, and E4.5) through uniform manifold approximation and projection (UMAP) clustering and marker expression, following the method as described by Lentini et al. (2022) (Figures S2A–S2C). As there were few XaXa cells in the late blastocyst, we used E5.5 XaXa epiblast cells (EPI:E5.5) as identified in our previous study (Naik et al., 2022). Next, we compared the allelic X:A ratio between $Xa^{mat}Xi^{pat}$ (EPI:ICM) and $Xa^{mat}Xa^{pat}$ (EPI:E5.5) cells (Figure 1A). Interestingly, we found that Xa^{mat}:A^{mat} ratio in $Xa^{mat}Xa^{pat}$ (EPI:E5.5) cells reduced significantly compared to the $Xa^{mat}Xi^{pat}$ (EPI:ICM) cells and reached close to 1, indicating the loss of Xa^{mat} upregulation in these cells (Figure 1A and Table S1). Next, we validated this directly through allelic expression analysis, which also showed no

Figure 1. Erasure of Xa upregulation upon reactivation of Xi in mouse embryonic epiblast

(A) Comparison of allelic X:A ratio (top) and allelic expression of X and autosomes (bottom) between EPI:ICM ($Xa^{mat}Xi^{pat}$) and EPI:E5.5 ($Xa^{mat}Xa^{pat}$) cells. A comparison between EPI:ICM and EPI:E5.5 epiblasts of male cells is also plotted.

(B) Comparison of allelic X(escapees):A ratio (left) and allelic expression of escapees and autosomes (right) between EPI:ICM ($Xa^{mat}Xi^{pat}$) and EPI:E5.5 ($Xa^{mat}Xa^{pat}$) cells.

(C) Heatmap representing the allelic expression changes of Xa^{mat} and Xi^{pat} genes upon transition of EPI:ICM ($Xa^{mat}Xi^{pat}$) cells to EPI:E5.5 ($Xa^{mat}Xa^{pat}$) cells. Xa^{mat}, maternal active-X; Xi^{pat}, paternal inactive-X. In all boxplots, the line inside each of the boxes denotes the median value, the red circle denotes the mean value, and the edges of each box represent 25% and 75% of the dataset, respectively (Wilcoxon rank-sum test: p values < *0.0001*; ****, < *0.01*; **, NS: not significant).

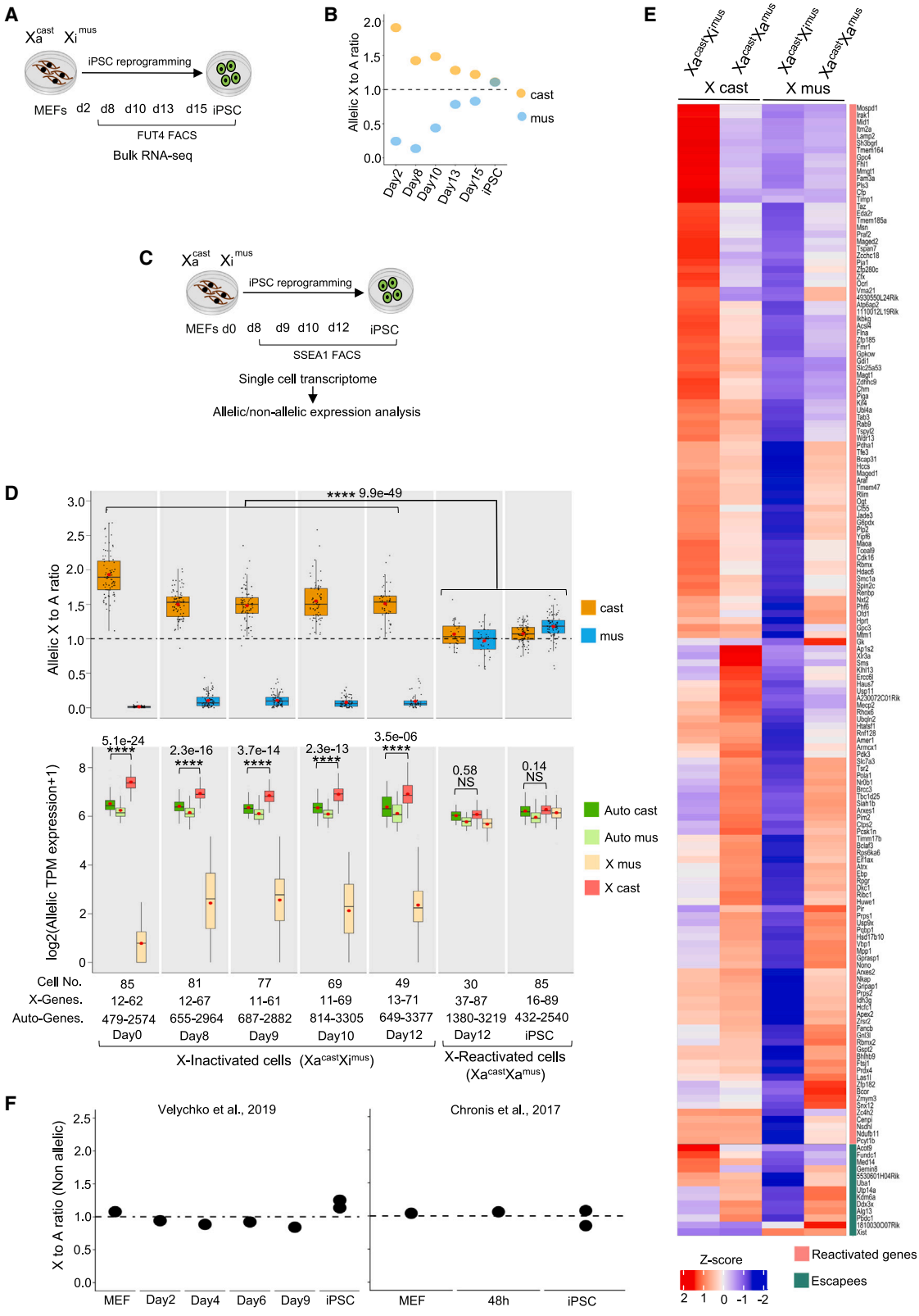

(legend on next page)

significant differences in expression between Xa^{mat} and A^{mat} allelic expression in $Xa^{mat}Xa^{pat}$ (EPI:E5.5) cells (Figure 1A). Analysis using a common set of genes among $Xa^{mat}Xa^{pat}$ vs. $Xa^{mat}Xi^{pat}$ cells corroborated our observations (Figures S2D and S2E). Next, we performed the aforementioned analysis with escapee genes only. Genes with fraction Xi^{pat} allele expression >0.10 in EPI:ICM ($Xa^{mat}Xi^{pat}$) cells were categorized as escapee genes (Figure S2F). We found that escapee genes also undergo upregulation in $Xa^{mat}Xi^{pat}$ (EPI:ICM) cells and upregulation is lost in $Xa^{mat}Xa^{pat}$ (EPI:E5.5) cells (Figure 1B). We would like to clarify that our escapee list can be confounded slightly with the genes undergoing reactivation at this stage. However, we found that many escapee genes identified belong to the escapees reported earlier in different mouse cells. Finally, allelic expression analysis of individual X-linked genes revealed that, indeed, the expression of many genes from the Xa^{mat} is reduced upon transition from $Xa^{mat}Xi^{pat}$ to $Xa^{mat}Xa^{pat}$ state (Figure 1C). Taken together, these analyses suggested the loss of Xa upregulation in female epiblast upon reactivation of the Xi. Overall, we found a positive correlation between the XCI and XCU across different stages of embryogenesis (Figure S2G). We extended our analysis to male cells as well. Surprisingly, we found that there is a reduction in Xa^{mat}:A^{mat} ratio in EPI:E5.5 cells compared to the EPI:ICM cells, albeit the Xa^{mat}:A^{mat} ratio was still close to 1.5 (Figure 1A). Importantly, the allelic expression analysis confirmed the presence of upregulated Xa in the EPI:E5.5 male cells (Figure 1A).

Loss of Xa upregulation upon reactivation of the Xi during mouse iPSC reprogramming

It is known that Xi genes get reactivated during the induced pluripotent stem cell (iPSC) reprogramming, and this reprogramming system has extensively been used to understand X chromosome dynamics (Bauer et al., 2021; Janiszewski et al., 2019; Maherali et al., 2007; Pasque et al., 2014; Talon et al., 2021). We investigated the status of Xa upregulation upon reactivation of Xi during the reprogramming of female mouse embryonic fibroblast (MEF) to iPSC. We used the available bulk RNA sequencing (RNA-seq) dataset of Oct4, Sox2, Klf4, and Myc-mediated iPSC reprogramming from the study by Janiszewski et al. (2019) (Figure 2A). These cells harbor polymorphic chromosomes originating from *Mus musculus* (mus) and cast strains, which allowed us to profile allelic expression (Figure 2A). Notably, these cells were pre-selected to have the X^{mus} as the Xi (Janiszewski et al., 2019). We analyzed day 2 MEF, different intermediate FUT4-positive cells (day 8, day 10, day 13, and day 15), and iPSCs (Figure 2A). We considered genes that showed >10 TPM expression for our analysis to exclude low-expressed genes. We found that Xa^{cast}:A^{cast} ratio in day 2 MEF was close to 2, indicating upregulation of Xa^{cast} (Figure 2B). Intriguingly, we found a gradual decrease in the Xa^{cast}:A^{cast} ratio from day 8 onward upon the increase in Xi^{mus}:A^{mus} ratio, suggesting concomitant loss of Xa^{cast} upregulation upon reactivation of Xi^{mus} (Figure 2B). Indeed, gene-wise analysis of reactivated genes (genes with fraction expression from X^{mus} >0.1 in XaXa iPSCs) revealed a decrease in the expression of many genes from Xa^{cast} in $Xa^{cast}Xa^{mus}$ iPSC compared to the $Xa^{cast}Xi^{mus}$ day 2 MEF cells (Figures S3A and S3B). Next, to get better insight, we extended our analysis to the single-cell level using the scRNA-seq dataset from Talon et al. (2021). These cells are hybrid (cast X mus), and inactivation is skewed toward the X^{mus} allele, which enabled us to profile allelic gene expression and distinguish expression from Xa^{cast} vs. Xi^{mus} (Figure 2C). We analyzed day 0 MEF, different intermediate SSEA1-positive cells (day 8, day 9, day 10, and day 12), and iPSCs (Figure 2C). First, we presumably identified X-inactivated ($Xa^{cast}Xi^{mus}$) and X-reactivated ($Xa^{cast}Xa^{mus}$) cells by profiling the fraction of allelic expression of X chromosomes throughout the different stages of reprogramming (Figures S3C and S3D). As expected, we found that day 0 MEF cells belonged to the X-inactivated category, whereas iPSC belonged to the X-reactivated category (Figure S3D). The majority of cells of day 8, day 9, day 10, and day 12 belonged to the X-inactivated category along with

Figure 2. Erasure of Xa upregulation upon reactivation of Xi during mouse iPSCs reprogramming

(A) Schematic showing different stages of reprogramming of female MEF to iPSC (bulk RNA-seq dataset).

(B) The plot represents allelic X:A ratio throughout the different stages of iPSC reprogramming.

(C) Schematic showing different stages of reprogramming of female MEF to iPSC (scRNA-seq dataset).

(D) Top: comparison of allelic X:A ratio between X-inactivated ($Xa^{cast}Xi^{mus}$) vs. X-reactivated ($Xa^{cast}Xa^{mus}$) cells during iPSC reprogramming. Bottom: allelic expression (log2 allelic TPM+1) of X-linked and autosomal genes in X-inactivated vs. X-reactivated cells during iPSC reprogramming (Wilcoxon rank-sum test: p value < *0.0001*; ****, NS: not significant).

(E) Heatmap representing the allelic expression changes of Xa^{cast} and Xi^{mus} genes upon conversion of X-inactivated ($Xa^{cast}Xi^{mus}$) cells to X-reactivated ($Xa^{cast}Xa^{mus}$) cells during iPSC reprogramming.

(F) Plots representing non-allelic X:A ratio throughout the different stages of reprogramming of male MEF to iPSC. In all boxplots, the line inside each of the boxes denotes the median value, the red circle denotes the mean value, and the edges of each box represent 25% and 75% of the dataset, respectively.

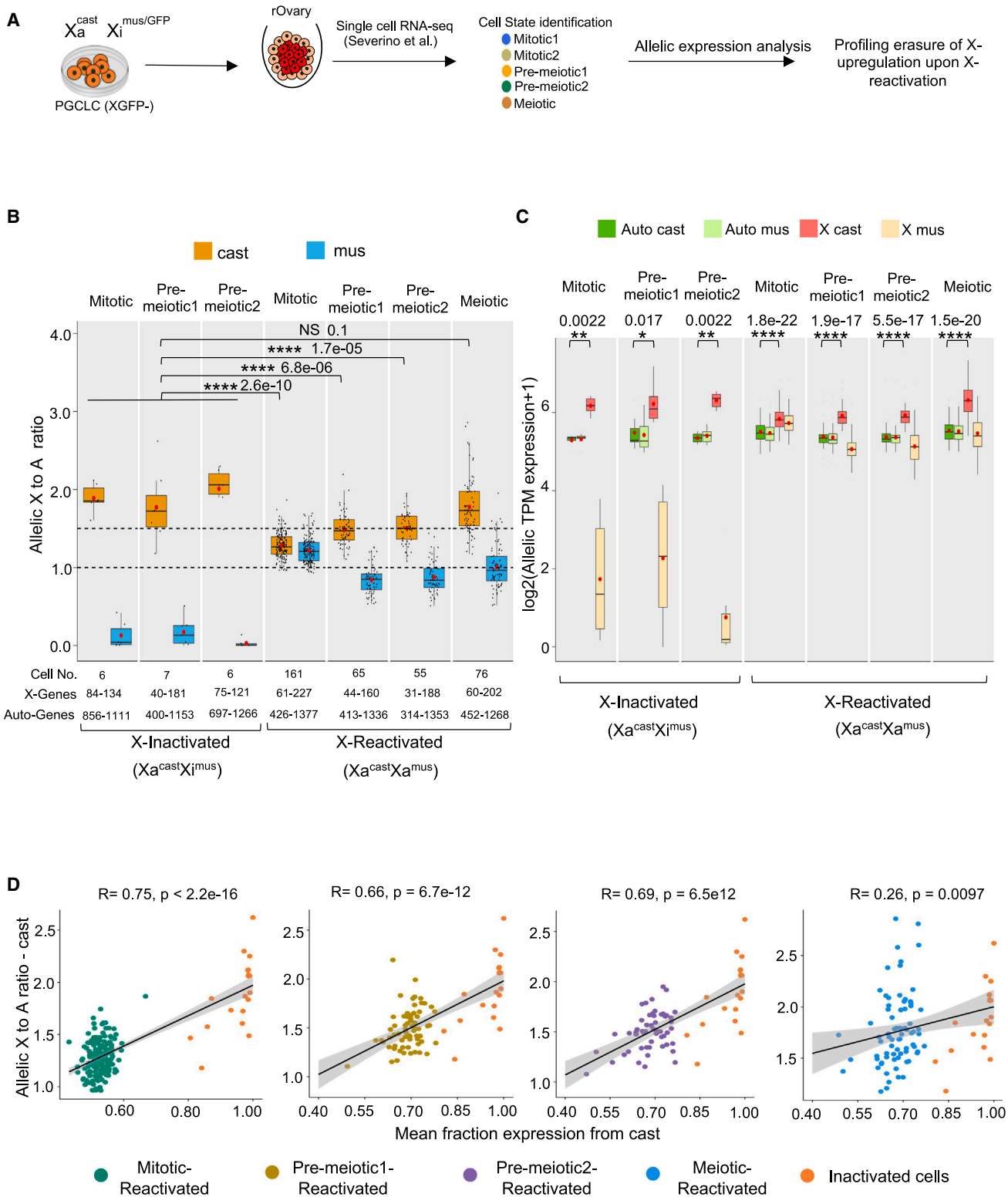

Figure 3. Reactivation of Xi and loss of Xa upregulation is not tightly coupled in mouse germ cells

(A) Schematic showing differentiation of XGFP- PGCLCs toward meiotic cells using rOvary system as described in the study by Severino et al., 2022 (Severino et al., 2022).

(legend continued on next page)

X-reactivated cells (Figure S3D). Next, we profiled allelic X:A ratio in these cells throughout the different stages of reprogramming. We found that Xa^{cast}:A^{cast} ratio in X-inactivated ($Xa^{cast}Xi^{mus}$) cells was >1.5 and close to 2, indicating Xa^{cast} upregulation (Figure 2D; Table S2). Interestingly, Xa^{cast}:A^{cast} ratio decreased significantly in X-reactivated ($Xa^{cast}Xa^{mus}$) cells and reached to ~1, suggesting the loss of Xa^{cast} upregulation in these cells (Figure 2D; Table S2). Allelic expression analysis of X-linked and autosomal genes also conferred the loss of X upregulation in X-reactivated ($Xa^{cast}Xa^{mus}$) cells (Figure 2D). Moreover, analysis of a common set of genes among X-inactivated vs. X-reactivated cells also recapitulated the loss of Xa^{cast} upregulation (Figures S4A and S4B). Next, we delineated the correlation between the loss of Xa^{cast} upregulation vs. reactivation of the Xi^{mus} by comparing the Xa^{cast}:A^{cast} ratio with the fraction expression from Xa^{cast} and we found a moderate positive correlation (r = 0.65), indicating Xi reactivation and loss of Xa upregulation are tightly coupled (Figure S4C). Next, we compared the allelic expression of individual reactivated X-linked genes between X-inactivated vs. X-reactivated cells (Figures S4D and 2E). As expected, we found that many X-linked genes showed a reduction in expression from the Xa^{cast} upon conversion from X-inactivated ($Xa^{cast}Xi^{mus}$) to X-reactivated ($Xa^{cast}Xa^{mus}$) state during reprogramming (Figure 2E). Escapee genes also showed a gradual loss of upregulation from the Xa^{cast} upon the gradual increase of their expression from the Xi^{mus} (Figure S4E). Altogether, our analysis suggested dynamic loss of Xa upregulation upon reactivation of the Xi during iPSC reprogramming. Our result is in line with previous findings, which showed that reactivation of the Xi is associated with the loss of Xa upregulation in mESC and ICM (Larsson et al., 2019; Lentini et al., 2022). On the other hand, we also profiled Xa expression dynamics during iPSC reprogramming in male cells through X:A ratio analysis using available bulk RNA-seq datasets (Chronis et al., 2017; Velychko et al., 2019) (Figure 2F). As expected, we find that male cells do not undergo such loss of Xa upregulation as observed in female cells (Figure 2F). Together, we conclude that the loss of Xa upregulation during iPSC reprogramming is female specific and primarily triggered by the reactivation of the Xi.

The reactivation of Xi and loss of Xa upregulation are not well coordinated in mouse germ cells

Germ cells are specified as primordial germ cells (PGCs) from the post-implantation epiblast of mouse embryo (Hajkova et al., 2002, 2008; Lawson et al., 1999). PGCs then migrate to the gonad, where they undergo sexual differentiation. During the migration, PGCs undergo extensive epigenetic reprogramming to erase the parental information and establish new marks during gametogenesis (Du et al., 2022; Hill et al., 2018). One such crucial epigenetic reprogramming that occurs in female PGCs is the reactivation of the Xi (Chuva De Sousa Lopes et al., 2008; Sangrithi et al., 2017; Severino et al., 2022; Sugimoto and Abe, 2007). However, whether the reactivation of Xi in germ cells leads to the loss of Xa upregulation remains poorly understood. Here, we have profiled the Xa expression dynamics during the reactivation of the Xi in germ cells at the single-cell level using the available scRNA-seq dataset of an *in vitro* germ cell differentiation system (Severino et al., 2022). In brief, Severino et al. derived primordial germ cell like cells (PGCLCs) from embryonic stem cells (ESCs) and differentiated PGCLCs to facilitate their meiotic entry using an *in vitro* reconstituted ovary (rOvary). rOvary was reconstituted through the aggregation of PGCLC and somatic cells from E13.5 embryonic gonad along with mesonephros to mimic female urogenital environment to facilitate the meiotic entry of germ cells (Hayashi et al., 2012). It has been shown that rOvary mimics the proper development of germ cells, including X reactivation, imprint erasure, and cyst formation (Hayashi et al., 2012). Importantly, Severino et al. have demonstrated that this *in vitro* PGCLC system recapitulates the heterogeneity and X chromosome dynamics of *in vivo* germ cell specification during the post-implantation development (Severino et al., 2022).

We analyzed scRNA-seq data of differentiated mouse germ cells, which originated from XGFP-negative PGCLC population as described in the study by Severino et al. (2022) (Figure 3A). XGFP-negative PGCLC population harbored inactivated X chromosome and underwent reactivation upon rOvary-mediated differentiation and thereby served as a good system to track the loss of Xa upregulation upon Xi reactivation. Additionally, these cells harbored polymorphic chromosomes from mus and cast origins,

(B) Comparison of allelic X:A ratio between X-inactivated ($Xa^{cast}Xi^{mus}$) and X-reactivated ($Xa^{cast}Xa^{mus}$) cells.
(C) Allelic expression (log2 allelic TPM+1) of X-linked and autosomal genes in X-inactivated ($Xa^{cast}Xi^{mus}$) vs. X-reactivated cells ($Xa^{cast}Xa^{mus}$).
(D) Scatterplots showing the correlation between Xa^{cast} upregulation (Xa^{cast}:A^{cast}) and reactivation of the Xi^{mus} (fraction expression from X^{cast} allele) in mitotic, pre-meiotic1, pre-meiotic2, and meiotic (labeled with different colors) germ cells. R is Pearson's correlation. In all boxplots, the line inside each of the boxes denotes the median value, the red circle denotes the mean value, and the edges of each box represent 25% and 75% of the dataset, respectively (Wilcoxon rank-sum test: *p* values < *0.0001*; ****, < *0.01*; ** and < *0.05*; *; NS: not significant).

thereby allowing us to profile allele-specific expression. Notably, X^{mus} is inactivated in these cells (Figure 3A). First, we segregated cells into mitotic and meiotic populations based on UMAP and marker-based clustering, as described by Severino et al. (2022) (Figure S5A). In consistency with Severino et al., we identified mitotic (mitotic 1 and 2), early meiotic (pre-meiotic 1 and 2), and late meiotic germ cells (Figures S5A and S5B). Next, we presumably categorized X-inactivated ($Xa^{cast}Xi^{mus}$) and X-reactivated ($Xa^{cast}Xa^{mus}$) cells by profiling the fraction allelic expression of X chromosomes (Figure S5C). We excluded low-expressed genes (<1 TPM) from our analysis. As expected, Xa^{cast}:A^{cast} ratio of X-inactivated ($Xa^{cast}Xi^{mus}$) cells of different stages was ~1.5–2, suggesting these cells harbor upregulated Xa (Figure 3B). However, we found that there was no reduction in Xa^{cast}:A^{cast} ratio in X-reactivated ($Xa^{cast}Xa^{mus}$) meiotic germ cells, indicating no loss of Xa upregulation in these meiotic cells upon X reactivation (Figure 3B and Table S3). To validate more, we compared the allelic expression of X chromosomes with the autosomal alleles of meiotic germ cells. Indeed, we found that like X-inactivated cells ($Xa^{cast}Xi^{mus}$), the expression of Xa^{cast} was significantly higher compared to the autosomal alleles in X-reactivated ($Xa^{cast}Xa^{mus}$) meiotic germ cells, corroborating the fact that there is no loss of Xa^{cast} upregulation in these cells (Figure 3C). Next, we performed gene-wise analysis for the reactivated genes (genes with fraction X^{mus} expression >0.10 in $Xa^{cast}Xa^{mus}$ cells, excluding escapees) (Figure S6D). We found that the majority of reactivated genes did not have a reduction in expression from the Xa^{cast} in X-reactivated ($Xa^{cast}Xa^{mus}$) pre-meiotic cells compared to the X-inactivated ($Xa^{cast}Xi^{mus}$) cells (Figure S7D). Only a subset of X-linked genes showed a mild reduction in Xa^{cast} expression (Figure S7D). Taken together, our analysis suggests that the reactivation of the Xi and the loss of Xa upregulation are not well coordinated in meiotic germ cells. On the other hand, we observed a significant reduction in Xa^{cast}:A^{cast} ratio in X-reactivated ($Xa^{cast}Xa^{mus}$) pre-meiotic cells compared to the X-inactivated ($Xa^{cast}Xi^{mus}$) cells (Figure 3B). However, we must mention that Xa^{cast}:A^{cast} was still quite high in X-reactivated pre-meiotic cells, indicating that the loss of Xa^{cast} upregulation is not robust in these cells. In fact, allelic expression analysis of X-linked and autosomal genes showed significantly higher expression of Xa^{cast} genes compared to the autosomal alleles in X-reactivated ($Xa^{cast}Xa^{mus}$) pre-meiotic cells, suggesting these cells are maintaining Xa upregulation despite the robust Xi reactivation (Figure 3C). We would like to mention that allelic expression analysis provides a better readout of Xa upregulation compared to the X:A ratio. Gene-wise analysis of the reactivated genes (Figures S6B and S6C) also showed that many genes do not have a reduction in expression from the Xa^{cast} in X-reactivated ($Xa^{cast}Xa^{mus}$) pre-meiotic cells compared to the X-inactivated cells ($Xa^{cast}Xi^{mus}$) (Figures S7B and S7C). Only a subset of X-linked genes showed a mild reduction in Xa^{cast} expression. On the other hand, X-reactivated mitotic cells showed a robust reduction in Xa^{cast}:A^{cast} ratio compared to the inactivated cells, although the Xa^{cast} expression was still quite high compared to the autosomal alleles, which was corroborated in gene-wise allelic expression analysis (Figures 3B, 3C, S6A, and S7A). However, we noticed slight hyperactivation of the Xi^{mus} allele in reactivated ($Xa^{cast}Xa^{mus}$) mitotic cells. Taken together, we conclude that loss of upregulation is partial, not complete, in the case of pre-meiotic and mitotic germ cells. Indeed, correlation analysis between loss of Xa upregulation vs. Xi reactivation showed a moderate correlation for mitotic or pre-meiotic germ cells (r = 0.66–0.75), whereas correlation was very much lower for meiotic germ cells (r = 0.26) (Figure 3D). To mitigate the variation in gene numbers in our scRNA-seq analysis, we repeated our X:A and allele-specific expression analysis using a common set of genes between X-inactivated vs. X-reactivated cells and found that overall observations remain consistent (Figure S8B and S8C). Similarly, analysis of mitotic 1 and mitotic 2 cells separately resulted in similar outcomes (Figure S8D). Interestingly, we found that most of the escapees undergo loss of Xa upregulation upon Xi reactivation in mitotic, pre-meiotic, and meiotic cells (Figures S8A and S6). Next, we explored if X reactivation timing contributes to the observed differences in pre-meiotic vs. meiotic gem cells. To explore that, we identified the late reactivating genes, which are reactivated in pre-meiotic 2 or meiotic cells but not in pre-meiotic 1 cells. However, we could identify only a few such genes and found that while few of them undergo loss of Xa upregulation, others do not (Figure S8E). We want to emphasize that our analysis is currently limited by low gene numbers, and therefore, it will be interesting to explore this aspect using the *in vivo* germ cell development dataset in the future. Collectively, we conclude that the loss of Xa upregulation upon Xi reactivation in pre-meiotic or meiotic germ cells is not well coordinated as it was observed for embryonic epiblast or iPSCs. It is worth discussing that *in vitro* re-capitulation of germ cell development may not faithfully illustrate the *in vivo* conditions, and therefore, more extensive study using an *in vivo* system can provide better clarity. On the other hand, we would like to mention that for analysis related to germ cells, we used genes from the following autosomes: Chr13, Chr9, Chr8, Chr7, and Chr5, as other autosomes are not fully hybrid in these cells. This was because the ESC line used for germ cell generation by Severino et al. was an F2 ESC line derived from a cross of mus with cast (Severino et al., 2022). Therefore, to be consistent, we repeated our analysis for the embryonic epiblast and iPSC data considering these autosomes only,

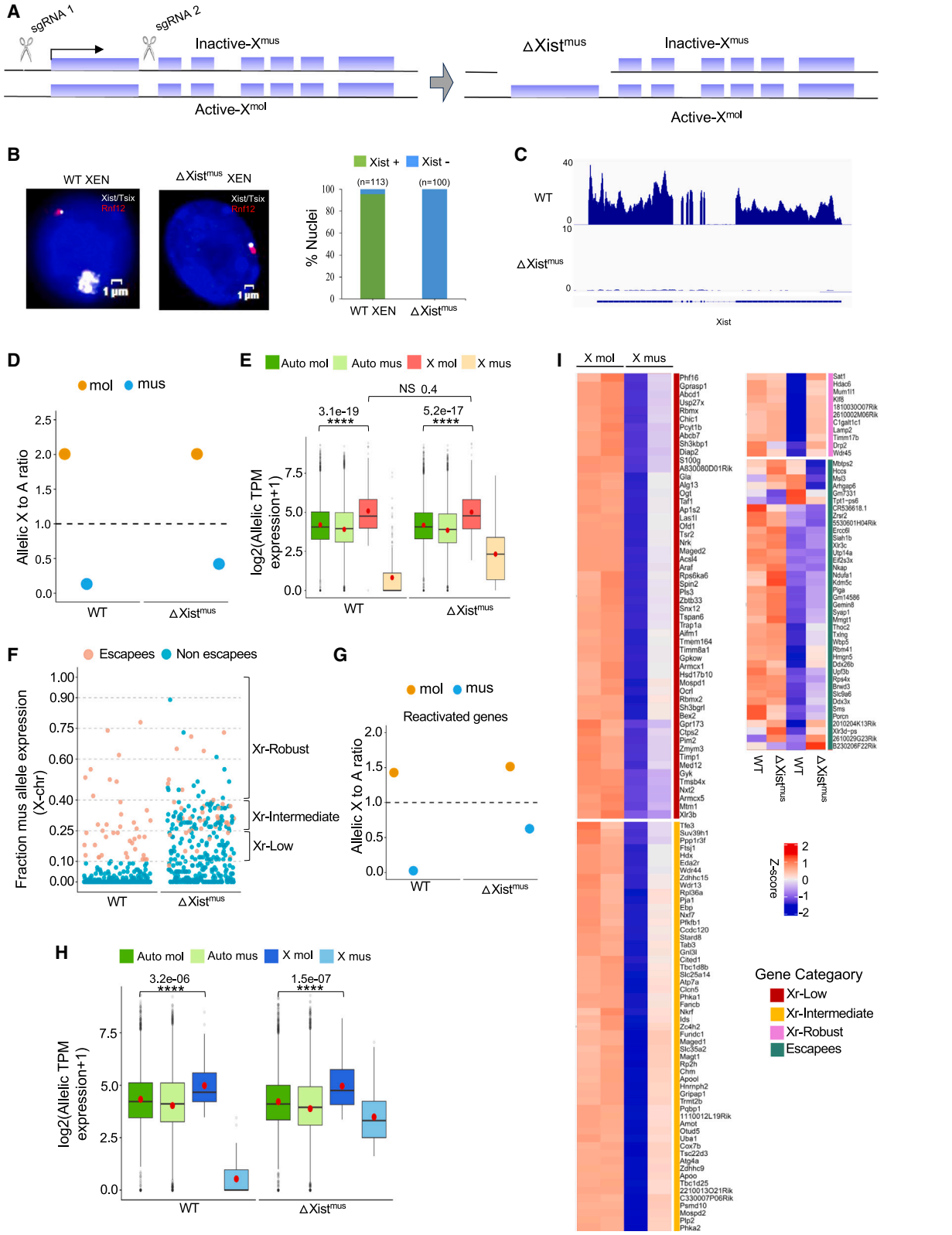

(legend on next page)

and we found that the overall results remained consistent (Figures S9A and S9B).

Partial reactivation of Xi in mouse XEN and human B cells does not trigger the loss of Xa upregulation

So far, in the aforementioned experiments, we investigated the loss of Xa upregulation in different lineages, which undergo spontaneous Xi reactivation. Next, we explored if the forced reactivation of Xi can trigger the loss of Xa upregulation in cell types that do not undergo Xi reactivation naturally. In a recent study, we showed that ablation of Xist in extra-embryonic endoderm (XEN) stem cells leads to the partial reactivation of Xi (Arava et al., 2023). Here, we explored if the reactivation of Xi genes in these cells leads to the loss of Xa upregulation. The XEN cells were derived from two divergent mouse strains, mus and *Mus Molassinus* (mol), allowing us to perform allele-specific gene expression analysis. Importantly, X inactivation is skewed toward paternal-X (X^{mus}) as XEN cells undergo imprinted X inactivation (Figure 4A). In these cells, Xist was deleted from paternal or Xi allele ($\Delta Xist^{mus}$) through a CRISPR-Cas9-based approach using two single-guide RNAs (sgRNAs) targeting the Xist upstream region and intron1, respectively (Figure 4A) (Arava et al., 2023). We validated the lack of Xist expression in this $\Delta Xist^{mus}$ XEN cell line using RNA-fluorescent *in situ* hybridization (RNA-FISH) and RNA-seq analysis (Figures 4B and 4C). Next, to track the reactivation and loss of Xa upregulation, we compared allelic X:A ratio between wild-type (WT) and $\Delta Xist^{mus}$ XEN cells using the allelic RNA-seq data. We found that while Xi^{mus}:A^{mus} ratio in WT XEN cells is close to zero, it increased to ~0.5 in $\Delta Xist^{mus}$ XEN (Figure 4D). Similarly, allelic expression analysis showed almost no expression of X-linked genes from the Xi^{mus} in WT cells; however, Xi gene expression increased in $\Delta Xist^{mus}$ XEN (Figure 4E). However, the increment was minimal and much lesser than the autosomal allelic expression, suggesting partial reactivation of the Xi (Figure 4E). However, we observed no differences in Xa^{mol}:A^{mol} ratio between WT and $\Delta Xist^{mus}$ XEN cells, indicating no loss of Xa upregulation (Figure 4D). Allelic expression analysis of X-linked and autosomal genes corroborated similar facts (Figure 4E). Next, we interrogated if homologous genes on the Xa of the reactivated genes undergo loss of Xa upregulation. To test this, first, we presumably identified different categories of reactivated genes (Xr-low, Xr-intermediate, and Xr-robust) based on the fraction allelic expression from the Xi (Figure 4F). Next, we compared allelic X:A ratio and allelic expression of these reactivated genes between WT and $\Delta Xist^{mus}$ XEN cells. We found that the Xa^{mol}:A^{mol} ratio for reactivated genes in WT XEN cells was close to 1.5, indicating these genes undergo upregulation; however, there was no change of this ratio in $\Delta Xist^{mus}$ XEN cells (Figure 4G). Similarly, allelic expression analysis showed significantly higher expression of these X-linked genes from Xa^{mol} allele compared to the autosomal allele in both WT and $\Delta Xist^{mus}$ XEN cells, indicating no loss of upregulation of these homologous genes on the Xa upon reactivation on the Xi (Figure 4H). Finally, we profiled the gene-wise allelic expression of different categories of reactivated genes in WT and $\Delta Xist^{mus}$ XEN cells, which revealed not much change in expression from the Xa upon reactivation (Figure 4I). Escapee genes also did not show a loss of Xa upregulation (Figure S9C). Taken together, our analysis revealed that forced partial reactivation of the Xi in $\Delta Xist^{mus}$ XEN cells does not result in the loss of Xa upregulation (Figure 5G).

Next, we extended our analysis to human B cells using available RNA-seq data (Yu et al., 2021). In these cells, Xi was reactivated by knocking down XIST through CRISPR interference (sgXIST) along with the treatment with DNMT and EZH2 inhibitors. Further, these cells have skewed X inactivation toward the paternal-X and, therefore, allowed us to differentiate the X-linked gene expression from Xa vs. Xi through allele-specific analysis. First, we performed allelic X:A ratio analysis in these cells and found that control B cells (Ctrl) harbor upregulated Xa as indicated by high (>1.5) Xa^{mat}:A^{mat} ratio (Figure 5A). On

Figure 4. Partial reactivation of Xi does not lead to the loss of active-X upregulation in mouse XEN cells

(A) Schematic showing the target sites of sgRNAs at the Xist locus and heterozygous deletion of Xist from the paternal Xi^{mus} allele.

(B) Left: detection of Xist/Tsix RNA (white) and Rnf12 (red) through RNA-FISH in WT and $\Delta Xist^{mus}$ XEN cells. DAPI stained the nuclei in blue. The scale bar represents 1 μm. Right: quantification of Xist-coated nuclei in WT and $\Delta Xist^{mus}$ XEN cells.

(C) RNA-seq signals for Xist in WT and $\Delta Xist^{mus}$ XEN cells.

(D) Plot representing the allelic X:A ratio in WT and $\Delta Xist^{mus}$ XEN cells.

(E) Plot representing autosomal and X chromosome allelic expression (Log2 allelic TPM+1) in WT and $\Delta Xist^{mus}$ XEN cells.

(F) Identification of different categories of reactivated genes (Xr-low, Xr-intermediate, and Xr-robust) based on the reactivation status through profiling the fraction Xi^{mus} allele expression in WT and $\Delta Xist^{mus}$ XEN cells.

(G) Allelic X:A ratio for reactivated X-linked genes in WT and $\Delta Xist^{mus}$ XEN cells.

(H) Allelic expression (log2 allelic TPM+1) plot for autosomal and reactivated X-linked genes in WT and $\Delta Xist^{mus}$ XEN cells.

(I) Heatmap representing the allelic expression changes of Xa^{mol} and Xi^{mus} genes (reactivated genes) of WT XEN cells upon partial reactivation of Xi in $\Delta Xist^{mus}$ XEN cells (Wilcoxon rank-sum test: p value < *0.0001*; ****; NS: not significant).

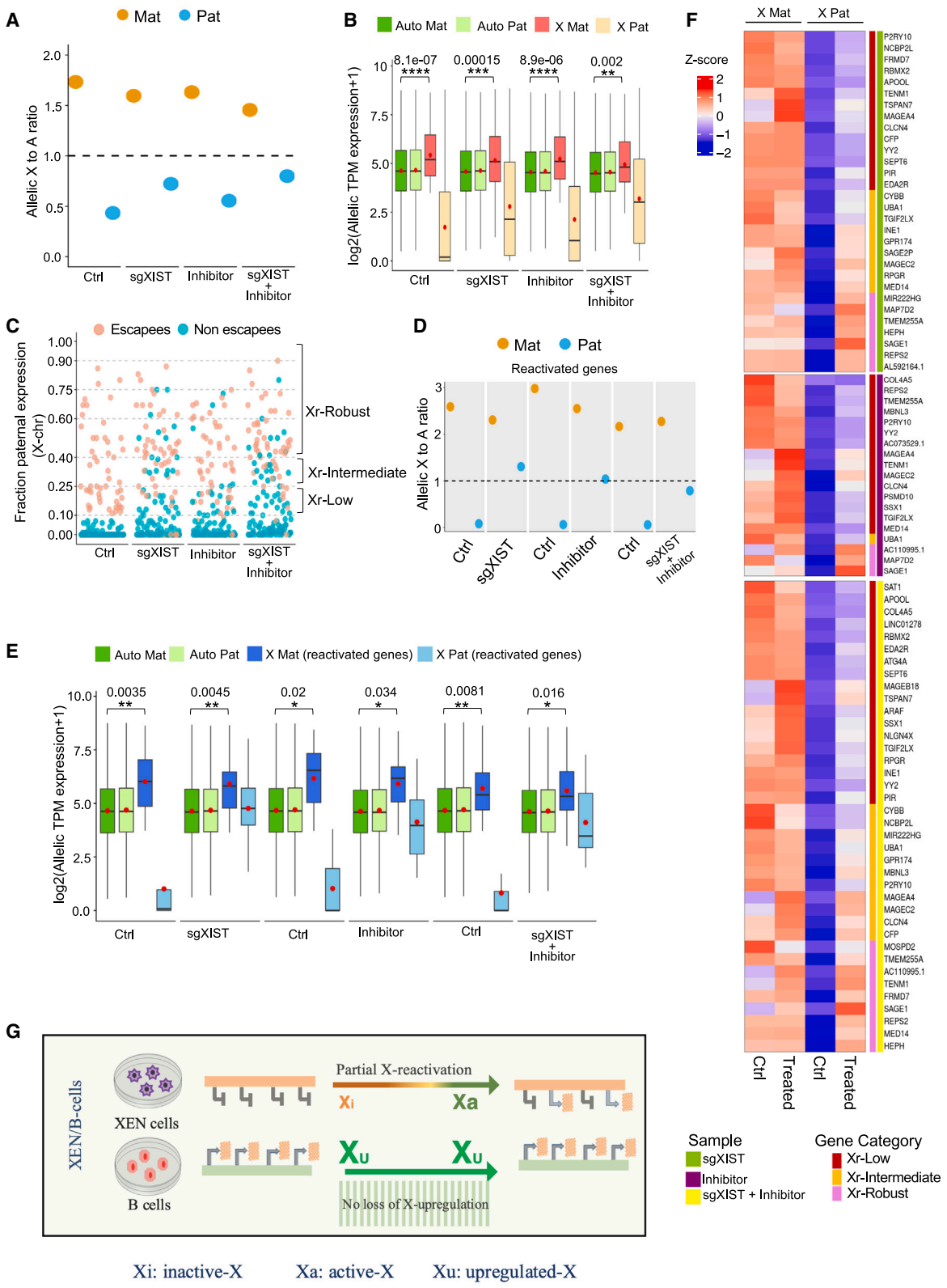

(legend on next page)

the other hand, in sgXIST, inhibitor-treated and sgXIST + inhibitor cells, there was a modest increase in Xi^{pat}:A^{pat} ratio compared to the Ctrl, indicating partial reactivation of the Xi (Figure 5A). However, there were not much changes in Xa^{mat}:A^{mat} ratio in these cells, suggesting no loss of Xa upregulation (Figure 5A). Allelic expression of X-linked and autosomal genes corroborated the similar facts (Figure 5B). Next, to be precise, we extended our analysis by focusing only on the reactivated genes. As described earlier, we identified different categories of reactivated genes (Xr-low, Xr-intermediate, and Xr-robust) through fraction allelic expression analysis of X chromosomes (Figure 5C). Allelic X:A ratio analysis of the reactivated genes cohort showed a slight reduction in Xa^{mat}:A^{mat} ratio in sgXIST, inhibitor-treated cells compared to the Ctrl cells (Figure 5D). However, we did not observe such a reduction in the case of sgXIST + inhibitor cells (Figure 5D). On the other hand, allelic expression analysis revealed that there was still higher Xa^{mat} expression compared to the autosomal allelic expression in sgXIST, inhibitor-treated and sgXIST + inhibitor cells (Figure 5E). Finally, gene-wise allelic expression analysis revealed that the majority of genes did not show a reduction in their expression from the Xa^{mat} in sgXIST, inhibitor-treated and sgXIST + inhibitor cells compared to the Ctrl cells (Figure 5F). Very few genes showed a slight reduction in expression from Xa^{mat} in sgXIST, inhibitor-treated and sgXIST + inhibitor cells. On the other hand, we observed that the expression of escapee genes from the Xa is higher compared to the corresponding autosomal allelic expression, indicating they undergo upregulation in B cells. These escapees maintained higher Xa expression compared to the autosomes in sgXIST, inhibitor-treated and sgXIST + inhibitor cells, although it was not significant in the case of sgXIST and sgXIST + inhibitor cells (Figure S9D). However, the gene-wise analysis did not show a loss of Xa upregulation for these escapees (Figure S9E). Overall, it appeared that in B cells, forced partial reactivation of the Xi does not trigger the loss of Xa upregulation (Figure 5G). For X upregulation analysis in both XEN and B cells, we analyzed those genes, which showed >10 TPM expression to exclude low-expressed genes.

Self-activation with cross-inhibitory regulation explains X chromosome dynamics during X reactivation

Next, we attempted to establish a phenomenological mathematical model to understand the nature of interactions between two X chromosomes during X chromosome reactivation. This is a simplified model where the expression levels of the X chromosomes are abstracted as nodes in a regulatory network. Our experimental data have shown dynamic erasure of X upregulation upon reactivation of the Xi during iPSC reprogramming. We simulated different alternative models and asked what nature of interactions between the two X chromosomes best explains the observed X chromosome dynamics during iPSC reprogramming based on mean allelic X:A ratio at different stages of reprogramming at the population level (Figure 2). We also tested different models in the context of partial reactivation as observed in $\Delta Xist^{mus}$ XEN cells (Figure 4). In this case, due to the lack of temporal data, we assumed a hypothetical case of iPSC reactivation stalling at day 12, and the value at day 12 was extrapolated up to day 15. These values match qualitatively with the partial reactivation state of $\Delta Xist^{mus}$ XEN cells. In our modeling framework, each X chromosome was considered a single entity, and we used the mean X:A ratio to represent the activity level for that particular X chromosome.

First, we verified the fits related to X:A ratio dynamics of the Xa and Xi chromosomes during iPSC reprogramming using antagonistic/inhibitory cross-regulation between the two chromosomes. We obtained poor fits, as represented in Figure 6A, suggestive of the fact that the model must be modified. The fits obtained by the addition of self-activations were much better than those without self-activations (Figure 6B). However, the fits obtained by the addition of self-inhibition were not satisfactory (Figure 6C). Similar exercises were done for the partial reactivation cases, for which the fits were better with self-activation as compared to the case of self-inhibition and no self-regulation (Figures 6D–6F). Taken together, this analysis indicated that some form of self-activatory

Figure 5. Partial reactivation of Xi in human B cells does not lead to the loss of X upregulation

Plots representing (A) allelic X:A ratio and (B) autosomal and X chromosome allelic expression (log2 allelic TPM+1) in Ctrl, sgXIST, inhibitor and sgXIST + inhibitor-treated B cells.

(C) Identification of different categories of reactivated genes (Xr-low, Xr-intermediate, and Xr-robust) based on the reactivation status through profiling of the fraction paternal X expression in Ctrl, sgXIST, inhibitor and sgXIST + inhibitor-treated B cells. Plots for (D) allelic X:A ratio for reactivated genes and (E) allelic expression (log2 allelic TPM+1) for autosomal and reactivated X-linked genes.

(F) Heatmap representing allelic expression of X-linked genes from Xi^{pat} and Xa^{mat} allele in Ctrl, sgXIST, inhibitor and sgXIST + inhibitor-treated B cells.

(G) Model representing that the partial reactivation of Xi does not result in loss of Xa upregulation in XEN and B cells. In all boxplots, the line inside each of the boxes denotes the median value and red circle mean value (Wilcoxon rank-sum test: *p* values < *0.0001*; ****, < *0.001*; ***, < *0.01*; ** and < *0.05*; *).

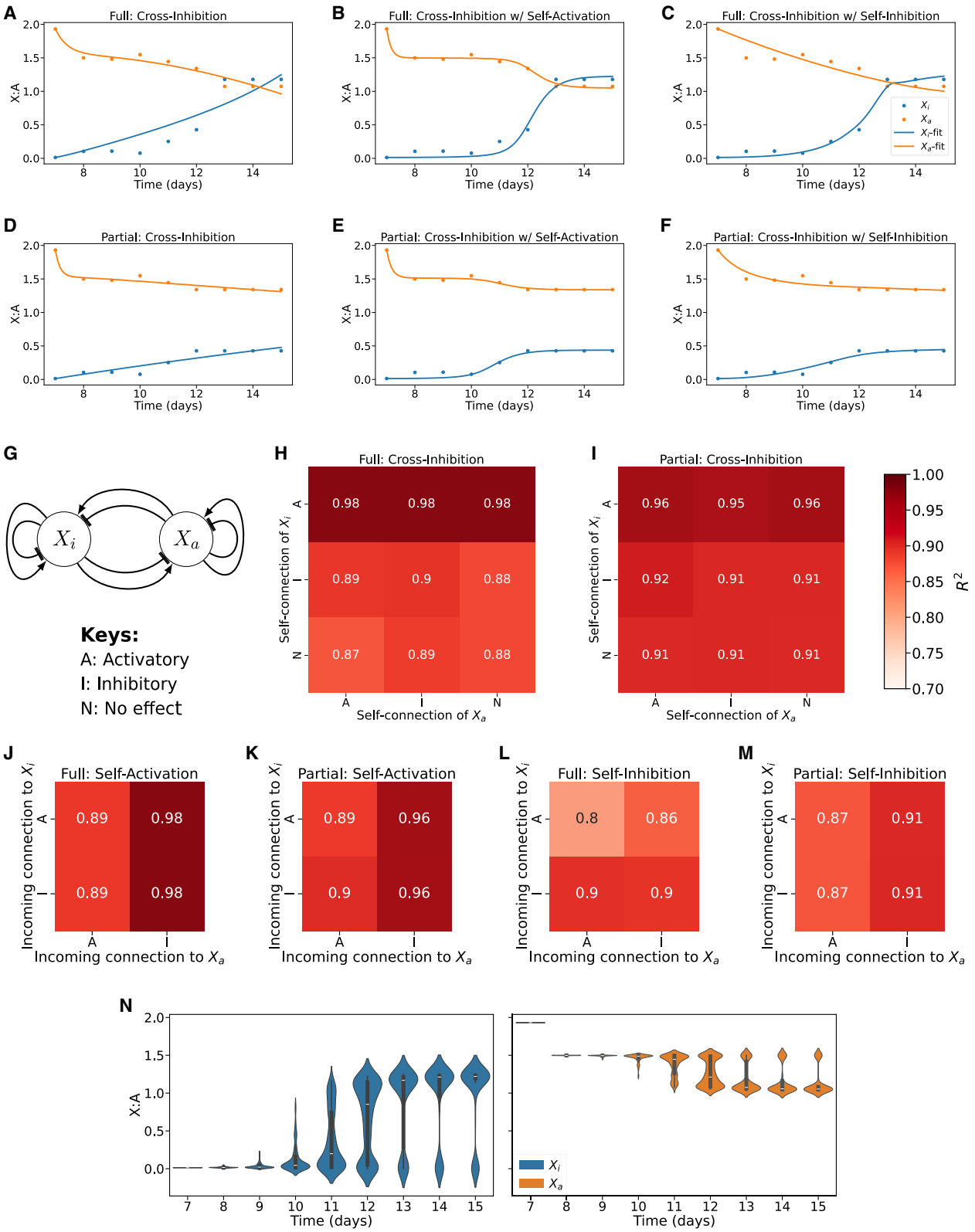

(legend on next page)

regulation is necessary to explain the observed X chromosome dynamics. Next, we considered all combinations of cross-regulatory links (interactions between the chromosomes) and self-regulatory links (interactions within a chromosome) (Figure 6G). We first tested the self-regulatory connections while the cross-regulatory connections were kept fixed as inhibitory. For both the full reactivation and partial reactivation cases, we observed that the connection to Xi being activatory gives a good fit regardless of the connection to Xi (Figures 6H and 6I) compared to the other cases. Next, we tested the cross-regulatory connections while fixing the self-regulatory connection as activatory. Here, we observed that the case that best fits both the full and partial reactivation case is when the incoming connection to Xa is inhibitory, while the incoming connection to Xi can be inhibitory or activatory (Figures 6J and 6K). Similarly, we also tested the cross-regulatory connections while fixing the self-regulatory connection to be inhibitory. We found that the incoming connection to Xa does not matter as much for the full reactivation case when the connection to Xi being inhibitory gives a better fit (Figure 6L). In the partial reactivation case, the incoming connection to Xa being inhibitory (Figure 6M) provides a relatively better fit, whereas the incoming connection to Xi does not matter as much. Altogether, our simulation results indicate that the self-activation with cross-inhibitory regulation better explains the X chromosome dynamics during reactivation of the Xi consistently for both partial and full reactivation. Our model so far has been fit to the mean X:A values at the population level. However, we observe heterogeneity in the population in the experimental data, i.e., at any time point, there is a fraction of the population having Xi (XaXi) and the others which initiated reactivation of the Xi (XaXa). Furthermore, this fraction keeps changing over time. We hypothesized that the heterogeneity can be explained by the presence of noise in the system. To test this hypothesis, we added a noise term to our equations and solved them with the parameter set we obtained from our fits. We see here that the addition of noise leads to a fraction of cells reactivating faster than the others in the system, evident by the bimodality (Figure 6N). Hence, our model, while phenomenological in nature and devoid of detailed mechanistic regulatory aspects, is sufficient to explain the heterogeneity in reactivation in addition to the mean behavior of the population.

DISCUSSION

In this study, we have explored the coordination of transcriptional output between two X chromosomes in female cells in different cellular/developmental contexts. We demonstrate that upon initiation of imprinted XCI in mouse pre-implantation embryos, there is concomitant upregulation from the Xa. Our result is consistent with a recent study by Lentini et al., (2022). Importantly, in line with the previous findings (Larsson et al., 2019; Lentini et al., 2022), we show that the reactivation of Xi in the embryonic epiblast cells is tightly coupled with the loss of Xa upregulation (Figure 1). Similarly, we find that the reactivation of Xi during iPSC reprogramming is associated with the dynamic loss of Xa upregulation (Figure 2). However, we find that the reactivation of the Xi in meiotic germ cells is not tightly coupled with the loss of Xa upregulation, suggesting that transcriptional states of two Xs are not always tightly linked; instead, it can occur in a lineage-specific manner (Figure 3). We acknowledge that our observation is based on an *in vitro* system that mimics the meiotic entry of PGCs, which may not fully represent the *in vivo* germ cell developmental dynamics and therefore, in the future, studying X chromosome dynamics *in vivo* can provide better clarity to this aspect. Indeed, a previous study indicated that the loss of X upregulation in germ cells *in vivo* is not coupled with the reactivation of X chromosome as the overall expression of X chromosomes was very high

Figure 6. Phenomenological model to explain partial and full reactivation dynamics

(A–F) Plots representing fits obtained from simulations related to X:A ratio of two X chromosomes during iPSC reprogramming: (A) with only cross-inhibition, (B) with cross-inhibition and self-activation, and (C) with cross-inhibition and self-inhibition. Plot representing fits on allelic X:A ratio during partial reactivation: (D) with only cross-inhibition, (E) with cross-inhibition and self-activation, and (F) with cross-inhibition and self-inhibition.

(G) Schematic representation of all combinations of possible cross-regulatory links (interactions between the chromosomes) and self-regulatory links (interactions within a chromosome).

(H and I) Heatmap representing R^2 for different fits for testing self-regulatory connections with fixed cross-inhibition on full and partial reactivation data, respectively.

(J and K) Heatmaps of R^2 for fits for testing cross-regulatory connections with fixed self-activation on full and partial reactivation data, respectively.

(L and M) Heatmaps of R^2 for fits testing cross-regulatory connections with fixed self-inhibition on full and partial reactivation data, respectively.

(N) Time-course distribution of X level on addition of noise to the model.

(Sangrithi et al., 2017). However, the study by Sangrithi et al. was not able to disentangle the expression between two X chromosomes at the individual cells as they lacked single-cell analysis as well as allele-based analysis. On the other hand, it may be possible that maintaining Xa upregulation is a prerequisite for achieving proper X chromosome dosage for meiotic entry of germ cells. Indeed, it has been reported that E12.5 to E14.5 mouse germ cells at the onset of meiotic entry have an excess dosage of X-linked gene expression (Sangrithi et al., 2017). Notably, oogenesis from XO or XY cells was not found to be efficient and coupled with several defects such as delayed entry to meiosis and progression, etc. (Hamada et al., 2020). Additionally, Severino et al. have shown that X chromosome states are important for efficient meiotic entry (Severino et al., 2022). In the future, more extensive studies are necessary to understand the relevance of the X chromosome state to PGC maturation. On the other hand, in the case of pre-meiotic germ cells, there may be a partial loss of X upregulation as the loss of upregulation was not complete or robust (Figures 3C and 3D). Collectively, we conclude that the coordination of transcriptional output of the two X chromosomes is not tightly coupled in germ cells as we observed for embryonic epiblast or iPSC reprogramming cells. It is worth discussing that it may be possible that although reactivation of the Xi in pre-meiotic germ cells was robust, it apparently looks a bit trailing behind from the completion, and that is why they do not show robust loss of Xa upregulation. However, our gene-wise analysis in germ cells showed robust reactivation of many X-linked genes, but not much erasure of X upregulation from the Xa chromosome (Figure S7). Moreover, in the case of iPSC reprogramming, even a bit of partial reactivation of the Xi in the X-inactivated cells category triggered the loss of Xa upregulation (Figure 2D). Together, in the future, more extensive analysis using *in vivo* germ cells is necessary to gain more insight into this aspect. On the other hand, mitotic germ cells showed loss of Xa upregulation upon Xi reactivation; however, we observed hyperactivation of both X chromosomes (Figures 3B and 3C). Together, our study uncovers that, while the transcriptional outputs of X-linked genes from the two Xs in mouse embryonic epiblast cells and iPSCs are tightly coordinated, that is not the case in germ cells.

On the other hand, we demonstrate that forced and partial reactivation of Xi in mouse XEN/human B cells is not associated with the loss of Xa upregulation either globally or from the homologous genes (Figure 5G). We must mention that forced reactivation in XEN/B cells was partial. Therefore, it could be possible that extensive chromosome-wide reactivation is necessary to trigger the loss of Xa upregulation, or these cell types lack the factors required for erasing Xa upregulation as they do not undergo the reactivation of Xi spontaneously. We would like to mention one caveat of our analysis that there could be a minute or partial loss of Xa upregulation upon partial reactivation of X-linked genes, which is difficult to capture in our current analysis. Indeed, we noticed that a few genes might be undergoing minor erasure or loss of upregulation from Xa upon Xi reactivation; however, they need to be investigated further in the future. Separately, it is worth mentioning that iPSCs, germ cells, and XEN cells used for our study were derived from a single cross. Therefore, it is possible that some of the allelic differences observed in our analysis could be due to the interspecies hybrid mice.

Separately, we have established a phenomenological mathematical model for transcriptional coordination of X chromosomes. We show that self-activation and the cross-inhibition between X chromosomes can provide a simplified explanation for the observed dynamics of X chromosomes during iPSC reprogramming (Figure 6). Notably, our model is in line with the elastic model of dosage compensation as described earlier (Lentini et al., 2022). However, it should be noted that this model suffers from the lack of high-resolution temporal data and might not have fully captured the inherent heterogeneity of the iPSC reprogramming system. Similarly, our model is phenomenological in nature and does not give a mechanistic basis, specifically the genetic and epigenetic factors involved in the regulation of X chromosome. Future iterations of this modeling framework can incorporate more specific molecular intermediaries in the process, enabling a better understanding of the key players. However, we believe this model will pave the path for future investigation of different molecular networks involved in such interactions. One possibility is that the cross-inhibition can be mediated through different *trans*-acting factors and/or competition between the two chromosomes for different *trans*-acting activators, as we reported previously during the initiation of random X inactivation (Naik et al., 2022). On the other hand, self-activation can be mediated through *cis*-acting repressors (Mutzel et al., 2019). Taken together, our study provides insights into X chromosome transcriptional dynamics in different developmental and cellular contexts and related mechanistic aspects.

EXPERIMENTAL PROCEDURES

Allele-specific RNA-seq analysis

We performed allele-specific analysis of RNA-seq data as described previously (Naik et al., 2021). In brief, we created an *in silico* reference genome by incorporating strain-specific SNPs into the mm10 reference genome. Strain-specific SNPs were obtained from the Mouse Genomes Project (https://www.sanger.ac.uk/science/data/mouse-genomes-project). Reads were mapped separately to

parental genomes using STAR. For removing any false positives in allelic count, we only considered those SNPs with minimum read counts of 10 (bulk RNA-seq data) and 3 (scRNA-seq data) per SNP site and used at least 2 informative SNPs per gene. We calculated allelic read counts by taking an average of SNP-wise reads. We normalized allelic read counts across cells using scaling factors obtained from DESeq2 using non-allelic count. The allelic ratio was calculated using the following formula: Allele-A or Allele-B/ Allele-A + Allele-B. Allelic TPM fraction (A or B) was calculated using the formula: Allelic ratio (A or B) * TPM of the gene. Here, Allele-A and Allele-B represents respective strains.

Visualization and plots

All plots were generated using R version 4.2.1 using ggplot2 library and Integrative Genomics Viewer for genome visualization.

All other experimental procedures can be found in the supplemental experimental procedures.

RESOURCE AVAILABILITY

Lead contact

Further information and requests should be directed to Dr. Srimonta Gayen: srimonta@iisc.ac.in.

Materials availability

This study did not generate any new unique reagents.

Data and code availability

RNA-seq data for XEN cells are available at Gene Expression Omnibus (GEO) with accession number: GEO: GSE273917 (Arava et al., 2023). The other previously published dataset used for this study is available at GEO under the following accessions: Pre-implantation embryos – GEO: GSE45719 (Deng et al., 2014), GEO: GSE80810 (Borensztein et al., 2017a), GEO: GSE89900 (Borensztein et al., 2017b), and GEO: GSE74155 (Chen et al., 2016); Post-implantation: GEO: GSE109071 (Cheng et al., 2019); iPSC: GEO: GSE153846 (Talon et al., 2021), GEO: GSE126229 (Janiszewski et al., 2019), GEO: GSE90894 (Chronis et al., 2017), and GEO: GSE137001 (Velychko et al., 2019); B cells: GEO: GSE164596 (Yu et al., 2021); and germ cells: GEO: GSE169201 (Severino et al., 2022). The code used for this study is available at https://github.com/Harshavardhan-BV/rev-XCI.

ACKNOWLEDGMENTS

We thank Prof. Sundeep Kalantry, University of Michigan, USA for reviewing the manuscript and providing BACs and cell lines. This study is supported by DBT grant (BT/PR30399/BRB/10/1746/2018), DST-SERB (CRG/2019/003067), DBT-Ramalingaswamy fellowship (BT/RLF/Re-entry/05/2016), and Infosys Young Investigator grant award to S.G. S.M., R.B., and A.M. acknowledge UGC or CSIR for the fellowship. H.BV. would like to acknowledge the Prime Minister Research Fellowship (PMRF), India. M.K.J. was supported by Ramanujan Fellowship (SB/S2/RJN-049/2018) by the SERB, Department of Science and Technology, Government of India, and by Param Hansa Philanthropies.

AUTHOR CONTRIBUTIONS

S.G. supervised and acquired the funding for the study. S.G. and H.C.N conceptualized the study. H.C.N performed all bioinformatic analysis. D.C., S.M., M.A., R.B., P.A., and A.M. performed experiments, data analysis, and result interpretation and assisted with conceptualization, experimental designing, and figure preparation. M.K.J., H.BV., and K.H. conceptualized and performed the simulation. S.G., H.C.N., S.M., M.A., M.K.J., H.BV., and K.H. wrote, edited, and proofread the manuscript. The final manuscript was edited and approved by all the authors.

DECLARATION OF INTERESTS

The authors declare no competing interests.

SUPPLEMENTAL INFORMATION

Supplemental information can be found online at https://doi.org/10.1016/j.stemcr.2024.10.001.

Received: March 11, 2024
Revised: October 1, 2024
Accepted: October 3, 2024
Published: October 31, 2024

REFERENCES

Arava, M., Majumdar, S., Bammidi, LS., Naik, HC., Baro, R., and Gayen, S. (2023). Gene-specific reactivation of X-linked genes upon Xist loss is linked to the chromatin states in extraembryonic endoderm and epiblast stem cells. Preprint at bioRxiv. https://doi.org/10.1101/2023.10.20.563299.

Bauer, M., Vidal, E., Zorita, E., Üresin, N., Pinter, S.F., Filion, G.J., and Payer, B. (2021). Chromosome compartments on the inactive X guide TAD formation independently of transcription during X-reactivation. Nat. Commun. *12*, 3499. https://doi.org/10.1038/S41467-021-23610-1.

Borensztein, M., Syx, L., Ancelin, K., Diabangouaya, P., Picard, C., Liu, T., Liang, J.B., Vassilev, I., Galupa, R., Servant, N., et al. (2017a). Xist-dependent imprinted X inactivation and the early developmental consequences of its failure. Nat. Struct. Mol. Biol. *24*, 226–233. https://doi.org/10.1038/nsmb.3365.

Borensztein, M., Okamoto, I., Syx, L., Guilbaud, G., Picard, C., Ancelin, K., Galupa, R., Diabangouaya, P., Servant, N., Barillot, E., et al. (2017b). Contribution of epigenetic landscapes and transcription factors to X-chromosome reactivation in the inner cell mass. Nat. Commun. *8*, 1297. https://doi.org/10.1038/s41467-017-01415-5.

Chen, G., Schell, J.P., Benitez, J.A., Petropoulos, S., Yilmaz, M., Reinius, B., Alekseenko, Z., Shi, L., Hedlund, E., Lanner, F., et al. (2016). Single-cell analyses of X Chromosome inactivation dynamics and pluripotency during differentiation. Genome Res. *26*, 1342–1354. https://doi.org/10.1101/gr.201954.115.

Chen, J., Wang, M., He, X., Yang, J.R., and Chen, X. (2020). The evolution of sex chromosome dosage compensation in animals. J. Genet. Genom. *47*, 681–693. https://doi.org/10.1016/J.JGG.2020.10.005.

Cheng, S., Pei, Y., He, L., Peng, G., Reinius, B., Tam, P.P.L., Jing, N., and Deng, Q. (2019). Single-Cell RNA-Seq Reveals Cellular Heterogeneity of Pluripotency Transition and X Chromosome Dynamics during Early Mouse Development. Cell Rep. *26*, 2593–2607.e3. https://doi.org/10.1016/j.celrep.2019.02.031.

Chronis, C., Fiziev, P., Papp, B., Butz, S., Bonora, G., Sabri, S., Ernst, J., and Plath, K. (2017). Cooperative Binding of Transcription Factors Orchestrates Reprogramming. Cell *168*, 442–459.e20. https://doi.org/10.1016/J.CELL.2016.12.016.

Chuva De Sousa Lopes, S.M., Hayashi, K., Shovlin, T.C., Mifsud, W., Surani, M.A., and McLaren, A. (2008). X Chromosome Activity in Mouse XX Primordial Germ Cells. PLoS Genet. *4*, e30. https://doi.org/10.1371/JOURNAL.PGEN.0040030.

Cidral, A.L., de Mello, J.C.M., Gribnau, J., and Pereira, L.V. (2021). Concurrent X chromosome inactivation and upregulation during non-human primate preimplantation development revealed by single-cell RNA-sequencing. Sci. Rep. *11*, 9624. https://doi.org/10.1038/s41598-021-89175-7.

Cloutier, M., Kumar, S., Buttigieg, E., Keller, L., Lee, B., Williams, A., Mojica-Perez, S., Erliandri, I., Rocha, A.M.D., Cadigan, K., et al. (2022). Preventing erosion of X-chromosome inactivation in human embryonic stem cells. Nat. Commun. *13*, 2516. https://doi.org/10.1038/S41467-022-30259-X.

Deng, Q., Ramsköld, D., Reinius, B., and Sandberg, R. (2014). Single-cell RNA-seq reveals dynamic, random monoallelic gene expression in mammalian cells. Science *343*, 193–196. https://doi.org/10.1126/science.1245316.

Deng, X., Hiatt, J.B., Nguyen, D.K., Ercan, S., Sturgill, D., Hillier, L.W., Schlesinger, F., Davis, C.A., Reinke, V.J., Gingeras, T.R., et al. (2011). Evidence for compensatory upregulation of expressed X-linked genes in mammals, Caenorhabditis elegans and Drosophila melanogaster. Nat. Genet. *43*, 1179–1185. https://doi.org/10.1038/ng.948.

Deng, X., Berletch, J.B., Ma, W., Nguyen, D.K., Hiatt, J.B., Noble, W.S., Shendure, J., and Disteche, C.M. (2013). Mammalian X upregulation is associated with enhanced transcription initiation, RNA half-life, and MOF-mediated H4K16 acetylation. Dev. Cell *25*, 55–68. https://doi.org/10.1016/j.devcel.2013.01.028.

Du, Z., Zhang, K., and Xie, W. (2022). Epigenetic Reprogramming in Early Animal Development. Cold Spring Harbor Perspect. Biol. *14*, a039677. https://doi.org/10.1101/CSHPERSPECT.A039677.

Graves, J.A.M. (2016). Evolution of vertebrate sex chromosomes and dosage compensation. Nat. Rev. Genet. *17*, 33–46. https://doi.org/10.1038/nrg.2015.2.

Gupta, V., Parisi, M., Sturgill, D., Nuttall, R., Doctolero, M., Dudko, O.K., Malley, J.D., Eastman, P.S., and Oliver, B. (2006). Global analysis of X-chromosome dosage compensation. J. Biol. *5*, 3. https://doi.org/10.1186/jbiol30.

Hajkova, P., Erhardt, S., Lane, N., Haaf, T., El-Maarri, O., Reik, W., Walter, J., and Surani, M.A. (2002). Epigenetic reprogramming in mouse primordial germ cells. Mech. Dev. *117*, 15–23. https://doi.org/10.1016/S0925-4773(02)00181-8.

Hajkova, P., Ancelin, K., Waldmann, T., Lacoste, N., Lange, U.C., Cesari, F., Lee, C., Almouzni, G., Schneider, R., and Surani, M.A. (2008). Chromatin dynamics during epigenetic reprogramming in the mouse germ line. Nature *452*, 877–881. https://doi.org/10.1038/nature06714.

Hamada, N., Hamazaki, N., Shimamoto, S., Hikabe, O., Nagamatsu, G., Takada, Y., Kato, K., and Hayashi, K. (2020). Germ cell-intrinsic effects of sex chromosomes on early oocyte differentiation in mice. PLoS Genet. *16*, e1008676. https://doi.org/10.1371/JOURNAL.PGEN.1008676.

Hayashi, K., Ogushi, S., Kurimoto, K., Shimamoto, S., Ohta, H., and Saitou, M. (2012). Offspring from oocytes derived from *in vitro* primordial germ cell-like cells in mice. Science *338*, 971–975. https://doi.org/10.1126/SCIENCE.1226889.

Hill, P.W.S., Leitch, H.G., Requena, C.E., Sun, Z., Amouroux, R., Roman-Trufero, M., Borkowska, M., Terragni, J., Vaisvila, R., Linnett, S., et al. (2018). Epigenetic reprogramming enables the transition from primordial germ cell to gonocyte. Nature *555*, 392–396. https://doi.org/10.1038/NATURE25964.

Huynh, K.D., and Lee, J.T. (2003). Inheritance of a pre-inactivated paternal X chromosome in early mouse embryos. Nature *426*, 857–862. https://doi.org/10.1038/nature02222.

Janiszewski, A., Talon, I., Chappell, J., Collombet, S., Song, J., De Geest, N., To, S.K., Bervoets, G., Marin-Bejar, O., Provenzano, C., et al. (2019). Dynamic reversal of random X-Chromosome inactivation during iPSC reprogramming. Genome Res. *29*, 1659–1672. https://doi.org/10.1101/GR.249706.119.

Kharchenko, P.V., Xi, R., and Park, P.J. (2011). Evidence for dosage compensation between the X chromosome and autosomes in mammals. Nat. Genet. *43*, 1167–1172. https://doi.org/10.1038/ng.991.

Larsson, A.J.M., Coucoravas, C., Sandberg, R., and Reinius, B. (2019). X-chromosome upregulation is driven by increased burst frequency. Nat. Struct. Mol. Biol. *26*, 963–969. https://doi.org/10.1038/s41594-019-0306-y.

Lawson, K.A., Dunn, N.R., Roelen, B.A., Zeinstra, L.M., Davis, A.M., Wright, C.V., Korving, J.P., and Hogan, B.L. (1999). Bmp4 is required for the generation of primordial germ cells in the mouse embryo. Genes Dev. *13*, 424–436. https://doi.org/10.1101/GAD.13.4.424.

Lentini, A., Cheng, H., Noble, J.C., Papanicolaou, N., Coucoravas, C., Andrews, N., Deng, Q., Enge, M., and Reinius, B. (2022). Elastic dosage compensation by X-chromosome upregulation. Nat. Commun. *13*, 1854. https://doi.org/10.1038/s41467-022-29414-1.

Li, X., Hu, Z., Yu, X., Zhang, C., Ma, B., He, L., Wei, C., and Wu, J. (2017). Dosage compensation in the process of inactivation/reactivation during both germ cell development and early embryogenesis in mouse. Sci. Rep. *7*, 3729. https://doi.org/10.1038/s41598-017-03829-z.

Lin, F., Xing, K., Zhang, J., and He, X. (2012). Expression reduction in mammalian X chromosome evolution refutes Ohno's hypothesis of dosage compensation. Proc. Natl. Acad. Sci. USA *109*, 11752–11757. https://doi.org/10.1073/pnas.1201816109.

Lin, H., Gupta, V., Vermilyea, M.D., Falciani, F., Lee, J.T., O'Neill, L.P., and Turner, B.M. (2007). Dosage compensation in the mouse balances up-regulation and silencing of X-linked genes. PLoS Biol. *5*, e326. https://doi.org/10.1371/JOURNAL.PBIO.0050326.

Lin, H., Halsall, J.A., Antczak, P., O'Neill, L.P., Falciani, F., and Turner, B.M. (2011). Relative overexpression of X-linked genes in mouse embryonic stem cells is consistent with Ohno's hypothesis. Nat. Genet. *43*, 1169–1172. https://doi.org/10.1038/ng.992.

Lyon, M.F. (1961). Gene Action in the X-chromosom of the mouse. Nature *190*, 372–373.

Lyu, Q., Yang, Q., Hao, J., Yue, Y., Wang, X., Tian, J., and An, L. (2022). A small proportion of X-linked genes contribute to X chromosome upregulation in early embryos via BRD4-mediated transcriptional activation. Curr. Biol. *32*, 4397–4410.e5. https://doi.org/10.1016/j.cub.2022.08.059.

Mahadevaiah, S.K., Sangrithi, M.N., Hirota, T., and Turner, J.M.A. (2020). A single-cell transcriptome atlas of marsupial embryogenesis and X inactivation. Nature *586*, 612–617. https://doi.org/10.1038/s41586-020-2629-6.

Maherali, N., Sridharan, R., Xie, W., Utikal, J., Eminli, S., Arnold, K., Stadtfeld, M., Yachechko, R., Tchieu, J., Jaenisch, R., et al. (2007). Directly Reprogrammed Fibroblasts Show Global Epigenetic Remodeling and Widespread Tissue Contribution. Cell Stem Cell *1*, 55–70. https://doi.org/10.1016/J.STEM.2007.05.014.

Mak, W., Nesterova, T.B., De Napoles, M., Appanah, R., Yamanaka, S., Otte, A.P., and Brockdorff, N. (2004). Reactivation of the Paternal X Chromosome in Early Mouse Embryos. Science *303*, 666–669. https://doi.org/10.1126/SCIENCE.1092674.

Mandal, S., Chandel, D., Kaur, H., Majumdar, S., Arava, M., and Gayen, S. (2020). Single-Cell Analysis Reveals Partial Reactivation of X Chromosome instead of Chromosome-wide Dampening in Naive Human Pluripotent Stem Cells. Stem Cell Rep. *14*, 745–754. https://doi.org/10.1016/j.stemcr.2020.03.027.

Marahrens, Y., Panning, B., Dausman, J., Strauss, W., and Jaenisch, R. (1997). Xist-deficient mice are defective in dosage compensation but not spermatogenesis. Genes Dev. *11*, 156–166. https://doi.org/10.1101/gad.11.2.156.

De Mello, J.C.M., Fernandes, G.R., Vibranovski, M.D., and Pereira, L.V. (2017). Early X chromosome inactivation during human preimplantation development revealed by single-cell RNA-sequencing. Sci. Rep. *7*, 1–12. https://doi.org/10.1038/s41598-017-11044-z.

Mutzel, V., Okamoto, I., Dunkel, I., Saitou, M., Giorgetti, L., Heard, E., and Schulz, E.G. (2019). A symmetric toggle switch explains the onset of random X inactivation in different mammals. Nat. Struct. Mol. Biol. *26*, 350–360. https://doi.org/10.1038/s41594-019-0214-1.

Naik, H.C., Hari, K., Chandel, D., Mandal, S., Jolly, M.K., and Gayen, S. (2021). Semicoordinated allelic-bursting shape dynamic random monoallelic expression in pregastrulation embryos. iScience *24*, 102954. https://doi.org/10.1016/J.ISCI.2021.102954.

Naik, H.C., Hari, K., Chandel, D., Jolly, M.K., and Gayen, S. (2022). Single-cell analysis reveals X upregulation is not global in pregastrulation embryos. iScience *25*, 104465. https://doi.org/10.1016/j.isci.2022.104465.

Nguyen, D.K., and Disteche, C.M. (2006). Dosage compensation of the active X chromosome in mammals. Nat. Genet. *38*, 47–53. https://doi.org/10.1038/NG1705.

Ohno, S. (1967). Sex Chromosomes and Sex-Linked Genes, *68* (Springer-Verlag), p. 1375. https://doi.org/10.7326/0003-4819-68-6-1375_2.

Okamoto, I., Otte, A.P., Allis, C.D., Reinberg, D., and Heard, E. (2004). Epigenetic Dynamics of Imprinted X Inactivation during Early Mouse Development. Science *303*, 644–649. https://doi.org/10.1126/SCIENCE.1092727.

Pasque, V., Tchieu, J., Karnik, R., Uyeda, M., Sadhu Dimashkie, A., Case, D., Papp, B., Bonora, G., Patel, S., Ho, R., et al. (2014). X chromosome reactivation dynamics reveal stages of reprogramming to pluripotency. Cell *159*, 1681–1697. https://doi.org/10.1016/j.cell.2014.11.040.

Pessia, E., Makino, T., Bailly-Bechet, M., McLysaght, A., and Marais, G.A.B. (2012). Mammalian X chromosome inactivation evolved as a dosage-compensation mechanism for dosage-sensitive genes on the X chromosome. Proc. Natl. Acad. Sci. USA *109*, 5346–5351. https://doi.org/10.1073/pnas.1116763109.

Sangrithi, M.N., Royo, H., Mahadevaiah, S.K., Ojarikre, O., Bhaw, L., Sesay, A., Peters, A.H.F.M., Stadler, M., and Turner, J.M.A. (2017). Non-Canonical and Sexually Dimorphic X Dosage Compensation States in the Mouse and Human Germline. Dev. Cell *40*, 289–301.e3. https://doi.org/10.1016/j.devcel.2016.12.023.

Schulz, E.G., Meisig, J., Nakamura, T., Okamoto, I., Sieber, A., Picard, C., Borensztein, M., Saitou, M., Blüthgen, N., and Heard, E. (2014). The two active X chromosomes in female ESCs block exit from the pluripotent state by modulating the ESC signaling network. Cell Stem Cell *14*, 203–216. https://doi.org/10.1016/j.stem.2013.11.022.

Severino, J., Bauer, M., Mattimoe, T., Arecco, N., Cozzuto, L., Lorden, P., Hamada, N., Nosaka, Y., Nagaoka, S.I., Audergon, P., et al. (2022). Controlled X-chromosome dynamics defines meiotic potential of female mouse *in vitro* germ cells. EMBO J. *41*, e109457. https://doi.org/10.15252/embj.2021109457.

Sugimoto, M., and Abe, K. (2007). X Chromosome Reactivation Initiates in Nascent Primordial Germ Cells in Mice. PLoS Genet. *3*, e116. https://doi.org/10.1371/JOURNAL.PGEN.0030116.

Takagi, N., and Sasaki, M. (1975). Preferential inactivation of the paternally derived X chromosome in the extraembryonic membranes of the mouse. Nature *256*, 640–642. https://doi.org/10.1038/256640a0.

Talon, I., Janiszewski, A., Theeuwes, B., Lefevre, T., Song, J., Bervoets, G., Vanheer, L., De Geest, N., Poovathingal, S., Allsop, R., et al. (2021). Enhanced chromatin accessibility contributes to X chromosome dosage compensation in mammals. Genome Biol. *22*, 302. https://doi.org/10.1186/s13059-021-02518-5.

Velychko, S., Adachi, K., Kim, K.P., Hou, Y., MacCarthy, C.M., Wu, G., and Schöler, H.R. (2019). Excluding Oct4 from Yamanaka Cocktail Unleashes the Developmental Potential of iPSCs. Cell Stem Cell *25*, 737–753.e4. https://doi.org/10.1016/J.STEM.2019.10.002.

Wang, F., Shin, J., Shea, J.M., Yu, J., Bošković, A., Byron, M., Zhu, X., Shalek, A.K., Regev, A., Lawrence, J.B., et al. (2016). Regulation of X-linked gene expression during early mouse development by Rlim. Elife *5*, e19127. https://doi.org/10.7554/eLife.19127.

Wang, M., Lin, F., Xing, K., and Liu, L. (2017). Random X-chromosome inactivation dynamics *in vivo* by single-cell RNA sequencing. BMC Genom. *18*, 90. https://doi.org/10.1186/s12864-016-3466-8.

Xiong, Y., Chen, X., Chen, Z., Wang, X., Shi, S., Wang, X., Zhang, J., and He, X. (2010). RNA sequencing shows no dosage compensation of the active X-chromosome. Nat. Genet. *42*, 1043–1047. https://doi.org/10.1038/ng.711.

Yang, J.R., and Chen, X. (2019). Dosage sensitivity of X-linked genes in human embryonic single cells. BMC Genom. *20*, 1–9. https://doi.org/10.1186/S12864-019-5432-8.

Yildirim, E., Sadreyev, R.I., Pinter, S.F., and Lee, J.T. (2011). X-chromosome hyperactivation in mammals via nonlinear relationships between chromatin states and transcription. Nat. Struct. Mol. Biol. *19*, 56–61. https://doi.org/10.1038/nsmb.2195.

Yu, B., Qi, Y., Li, R., Shi, Q., Satpathy, A.T., and Chang, H.Y. (2021). B cell-specific XIST complex enforces X-inactivation and restrains atypical B cells. Cell *184*, 1790–1803.e17. https://doi.org/10.1016/j.cell.2021.02.015.

Zhang, H., Gayen, S., Xiong, J., Zhou, B., Shanmugam, A.K., Sun, Y., Karatas, H., Liu, L., Rao, R.C., Wang, S., and Nesvizhskii, A.I. (2016). MLL1 Inhibition Reprograms Epiblast Stem Cells to Naive Pluripotency Article MLL1 Inhibition Reprograms Epiblast Stem Cells to Naive Pluripotency. Cell Stem Cell *18*, 481–494. https://doi.org/10.1016/j.stem.2016.02.004.